

PAPER

View Article Online  
View Journal | View Issue



Cite this: *Environ. Sci.: Nano*, 2025, 12, 3565

# Environmental behavior, hazard and anti-corrosion performance of benzotriazole-based nanomaterials for sustainable maritime applications†

Joana Figueiredo,<sup>a</sup> Fernando Perina,<sup>b</sup> Diana Carneiro,<sup>iD</sup><sup>b</sup> Muhammad Ahsan Iqbal,<sup>c</sup> Tânia Oliveira,<sup>d</sup> Cláudia Rocha,<sup>d</sup> Frederico Maia,<sup>d</sup> João Tedim<sup>iD</sup><sup>c</sup> and Roberto Martins<sup>iD</sup><sup>\*b</sup>

Metal corrosion is a colossal technical, economic, and environmental challenge worldwide. Protective coatings containing corrosion inhibitors (CIs) are commonly used to address this natural process, particularly severe in immersed structures in seawater. However, high-performance CIs, such as benzotriazole (BTA), often exhibit toxicity towards aquatic organisms and leach prematurely. This study introduces safe and sustainable-by-design engineered nanomaterials, specifically layered double hydroxides loaded with BTA (Mg–Al LDH–BTA and Zn–Al LDH–BTA), as an innovative and eco-friendly approach compared to state-of-the-art CIs. This study aims to characterize both nanomaterials, assess their anti-corrosion performance when incorporated in polyurethane coatings, and evaluate their environmental behavior when dispersed in water, short-term acute and chronic effects on temperate marine species, and the environmental hazard. Key findings include a superior anti-corrosion performance of coatings containing Zn–Al LDH–BTA compared to BTA-coatings. Aqueous dispersions of nanomaterials exhibit instability of particle size and zeta potential over time, while concentrations of metals (Al, Zn) and nitrates reach high levels in the highest tested concentration due to partial dissolution, which may explain the observed toxicity patterns (median effect concentrations in the mg L<sup>-1</sup> range). The tested compounds were not toxic for most tested species, apart from bacteria (*Aliivibrio fischeri*) and/or echinoderms (*Paracentrotus lividus*) and, in case of Mg–Al LDH–BTA, also on two microalgae species. The highest statistical PNEC value was observed for Mg–Al LDH–BTA (PNEC = 0.326 mg BTA per L), while the highest deterministic PNEC value was found for Zn–Al LDH–BTA (PNEC = 0.00041 mg BTA per L). These findings indicate that both nanomaterials are environmentally sound and efficient alternatives for anti-corrosion maritime applications.

Received 30th September 2024,  
Accepted 2nd June 2025

DOI: 10.1039/d4en00919c

rsc.li/es-nano

## Environmental significance

Corrosion is one of the most challenging problems for maritime industry. State-of-the-art solutions often rely on coatings containing toxic corrosion inhibitors that leach prematurely. A novel approach involves immobilizing corrosion inhibitors (*e.g.*, benzotriazole – BTA) within layered double hydroxides (LDH), offering controlled release under specific conditions with environmental benefits. This study presents a comprehensive assessment of the anti-corrosion performance, environmental behavior, ecotoxicity and hazard of novel BTA-based nanomaterials. These findings offer crucial insights for understanding and managing the environmental risks of emerging nanomaterials. Overall, the new nanomaterials enhance the corrosion protection of coatings while being less harmful to marine species compared to the state-of-the-art soluble corrosion inhibitor (BTA). Therefore, this technique seems a promising alternative for developing more efficient and green corrosion inhibitors with clear environmental benefits.

<sup>a</sup> Department of Biology, University of Aveiro, 3810-193 Aveiro, Portugal

<sup>b</sup> CESAM-Centre for Environmental and Marine Studies and Department of Biology, University of Aveiro, 3810-193 Aveiro, Portugal. E-mail: roberto@ua.pt

<sup>c</sup> CICECO-Aveiro Institute of Materials and Department of Materials and Ceramic Engineering, University of Aveiro, 3810-193 Aveiro, Portugal

<sup>d</sup> Smallmatek, Small Materials and Technologies, 3810-075 Aveiro, Portugal

† Electronic supplementary information (ESI) available. See DOI: <https://doi.org/10.1039/d4en00919c>

## 1. Introduction

Corrosion arises from the chemical/electrochemical reactions between metals and their surrounding environment, naturally leading to the deterioration or weakening of structures where these materials are used.<sup>1,2</sup> Alloyed metals, such as steel, are particularly susceptible to corrosion and



increased susceptibility to damage, especially when exposed to aggressive substances like seawater.<sup>3,4</sup> Without effective management, corrosion can disrupt production in industrial facilities, compromise the integrity of offshore structures, result in structural failure and, ultimately, human casualties.<sup>5</sup> Depending on the country, annual expenses for corrosion may vary between 1% and 5% of the gross domestic product, to ensure adequate protection of metallic structures from corrosion and enhance their stability and longevity.<sup>6,7</sup> The implementation of corrosion management measures has the potential to result in a reduction of up to 20% in expenses, covering both direct and indirect costs associated with its effects.<sup>7</sup>

Several approaches have been adopted to mitigate corrosion, including the use of suitable metals or alloys that are resistant to corrosion, applying laser technology to enhance the corrosion resistance of metals, implementing cathodic or anodic protection techniques, the application of polymeric coatings or the integration of corrosion inhibitors (CIs) into protective coatings.<sup>8–11</sup> Among these, the application of polymeric coatings combined with cathodic protection and corrosion inhibitors has demonstrated superior performance in terms of corrosion.<sup>2,12–14</sup> Traditionally, marine coatings incorporated anticorrosion pigments, with chromate-based ones among the most effective ones.<sup>15</sup> However, their toxicity<sup>16,17</sup> led to the ban of their use in maritime applications.<sup>15,18,19</sup> Moreover, incorporating directly alternative CIs (*e.g.* organic molecules) which are less (but still) toxic into coatings has demonstrated additional several drawbacks, including: (a) unfavorable interactions between the inhibitors and the coating matrix,<sup>20</sup> leading to material degradation<sup>21</sup> and (c) the premature uncontrolled release of CIs into the environment, resulting in reduced protective longevity.<sup>22–24</sup> These challenges underscore the necessity of seeking eco-friendly and effective alternatives to conventional inhibitors.

More recently, the immobilization of CIs into “smart” engineered nanomaterials has been suggested as one promising alternative to overcome the aforementioned challenges.<sup>13,25,26</sup> In the present study, the immobilization of the commercial corrosion inhibitor benzotriazole (BTA; CAS no.: 95-14-7; Sigma-Aldrich®) in the layered double hydroxides (LDHs) (particularly Mg–Al LDH and Zn–Al LDH) is being proposed as a substitute for the direct addition of CIs into the coatings. BTA is a heterocyclic compound that has proven to be an effective corrosion inhibitor for copper and its alloys, stainless steel, copper steel, and brass.<sup>27–31</sup> BTA was not yet classified by the European Chemical Agency (ECHA), but in the substance infocard, it is regarded as toxic to aquatic life with long-lasting effects, according to the classification provided by companies.<sup>17</sup> LDHs, also referred to as engineered hydrotalcite nanoclays, are characterized by their lateral dimensions, typically within the range of 20 to 40 nm, and are distinguished by their customizable physicochemical characteristics.<sup>32–35</sup> They can be synthesized with a variety of metal ions integrated into their structure, which consists of positively charged metal hydroxide layers (*e.g.*, Zn<sup>2+</sup> and Al<sup>3+</sup>) stabilized by anions such as NO<sub>3</sub><sup>–</sup>,

along with water molecules.<sup>13,36</sup> Other notable features of LDHs include their self-healing ability, strong adhesion to substrates, and the capability for anion exchange, allowing the controlled release of corrosion inhibitors while entrapping corrosive agents like chloride ions, thereby enhancing their protective performance.<sup>37,38</sup> LDHs are considered as ‘smart’ or stimuli-responsive nanomaterials due to their ability to undergo specific, controlled physicochemical changes in response to external stimuli, such as variations in pH, temperature, or the presence of aggressive ions. This adaptive behavior enables LDHs to play a critical role in applications such as corrosion protection, drug delivery, and environmental remediation.<sup>39–41</sup> LDHs have been indicated as being no/low toxic to marine and freshwater species.<sup>25,42,43</sup> In addition, several studies demonstrated that LDHs are effective nanocontainers for various active compounds, including anti-fouling biocides (such as DCOIT, Zn and Cu pyrithiones), colorimetric sensors, and corrosion inhibitors (such as MBT, vanadates and phosphates).<sup>44–46</sup> The immobilization of the active ingredients in LDHs allowed their controlled release over time, increased anti-corrosion efficacy, and decreased toxicity compared to their soluble forms.<sup>13,25,37,38</sup>

Several studies have investigated Zn–Al or Mg–Al LDHs intercalated with BTA (Fig. 1), with a particular emphasis on their anti-corrosion properties.<sup>47–50</sup> The incorporation of BTA into the LDH structure has been shown to significantly enhance the corrosion resistance of metal substrates.<sup>47–50</sup> Analytical techniques such as ultraviolet-visible (UV-vis) spectroscopy and X-ray diffraction (XRD) have demonstrated that BTA is released in response to the presence of chloride ions, which are simultaneously captured by the LDH matrix.<sup>47–49</sup> This mechanism not only facilitates the controlled release of the inhibitor but also reduces the availability of chloride ions.<sup>48,49</sup> Scanning electron microscopy (SEM) combined with energy-dispersive spectroscopy (EDS) has further confirmed the release of BTA from the LDH and the formation of protective complexes specifically at corrosion sites.<sup>49</sup> Electrochemical impedance spectroscopy (EIS) has revealed increased impedance values, while polarization studies have shown a reduction in corrosion rates, supporting the ENMs active inhibition performance.<sup>47–49</sup>

However, Zn–Al LDH–BTA and Mg–Al LDH–BTA are still relatively underexplored, particularly concerning their toxicity and environmental behavior but are being considered for industrial applications considering their prospective anticorrosion properties. In this context, the present work aimed to provide a comprehensive characterization of both ENMs, show their application as anticorrosive pigments when incorporated in polyurethane coatings, study their environmental behavior in aqueous dispersions and providing the first insights on their short-term acute and chronic effects on marine species, and environmental hazard in the marine compartment. Results will be compared to the soluble form of BTA under the hypothesis that both “smart” (*i.e.*, stimuli-responsive) nanomaterials demonstrate better or at least similar anti-corrosion and environmental performance. Hence, this study offers valuable insights on a novel strategy for addressing



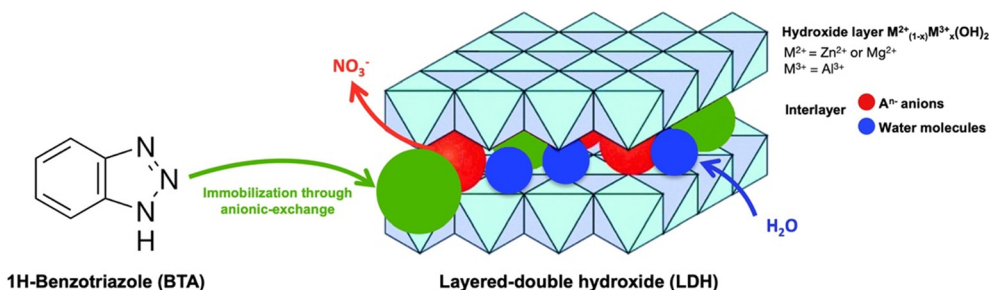


Fig. 1 Schematic illustration of layered double hydroxides (LDHs) structure, chemical components, and intercalation with benzotriazole (BTA).

a significant challenge in industrial sustainability, namely the development of environmentally friendly anti-corrosion materials and coatings. It provides key data on the characterization, toxicity, and potential hazards associated with Zn/Mg–Al LDH–BTA, supporting future risk assessment. Furthermore, the present work promotes the transition toward safer and more sustainable anti-corrosion solutions by demonstrating how industrial performance can align with environmental safety.

## 2. Materials and methods

### 2.1. Nanomaterials synthesis

Two initial LDH precursors, Zn–Al LDH– $NO_3$  and Mg–Al LDH– $NO_3$ , were synthesized using the co-precipitation method. To produce stable layered compounds, a  $M(II):M(III)$  ratio of 2:1 was chosen.<sup>13</sup> In this process, 200 mL of a solution containing 0.5 M  $Zn(NO_3)_2$  or  $Mg(NO_3)_2$  and 0.25 M  $Al(NO_3)_3$  was gradually added to 400 mL of a 1.5 M  $NaNO_3$  solution (pH = 8.5), over a 2 h period under vigorous stirring at room temperature. The pH was maintained at 8.5 using a 2 M NaOH solution. The resulting slurry underwent hydrothermal treatment at 100 °C for 4 h to induce LDH crystallization. Subsequently, the product was centrifuged and washed three times with boiled distilled water. A portion of the LDHs was dried at 60 °C for analysis, while the remaining material was employed in an anion-exchange reaction to substitute nitrate ( $NO_3^-$ ) by BTA<sup>−</sup> anions. The Zn–Al LDH– $NO_3$  and Mg–Al LDH– $NO_3$  slurries were dispersed in a 0.1 M solution of BTA (pH = 7.4) and stirred vigorously for 48 h. The resulting products, Zn–Al LDH–BTA and Mg–Al LDH–BTA were centrifuged and washed three times with boiled distilled water, with a small fraction of the LDHs dried at 60 °C for analysis.

### 2.2. Characterization of engineered nanomaterials

**2.2.1. Physical and chemical properties.** The morphology was assessed through scanning electron microscopy (SEM) using a Hitachi S-4100 system operating at an electron beam energy of 15 kV and coupled with energy dispersive spectroscopy (EDS).

The powder XRD characterization of the obtained nanomaterials was performed at room temperature, using a PANalytical X'Pert Powder diffractometer (CuK $\alpha$ 1 radiation,  $\lambda$  = 0.154056 nm; a tube power of 45 kV and 40 mA) coupled

with a PIXcell1D detector, and with a step of 0.02° over an angular range (2  $\theta$ ) between 3.5° and 75°.

For the chemical properties characterization of the nanomaterials, Fourier transform infrared spectroscopy (FTIR) spectra were obtained using a Perkin Elmer Spectrum Two spectrometer equipped with a UATR TWO unit (Diamond). The spectra were collected with 64 scans, a resolution of 4  $cm^{-1}$  and in a wavelength range of 400–4000  $cm^{-1}$ .

**2.2.2. Preparation and anti-corrosion properties of polyurethane coatings with BTA-based corrosion inhibitors.** To improve our understanding of the behavior and efficacy of the nanomaterials when incorporated in polyurethane coatings for high-performance applications, Zn–Al LDH–BTA was chosen as a nanostructured anti-corrosion pigment for corrosion studies. A polyurethane coating containing only BTA was similarly formulated to compare its performance against its soluble counterpart.

Regarding the coating composition, the basic polymeric coating was a commercial two-component polyurethane (provided by Synpo a.c.) consisting of the lacquer AQ CC 150 and the hardener AQ BU 13, with respective mass ratios of 2.5:1. This formulation was subsequently modified by incorporating BTA additives in two forms: directly as soluble CI (BTA) and as a nanostructured form (Zn–Al LDH–BTA). For this purpose, PU coatings containing 3 wt% BTA or LDH–BTA were prepared by adding them to polyurethane resin and dispersing them using ultrasonic vibration and mechanical stirring. The polyurethane coating with the desired thickness of 200  $\mu m$  was then applied onto the degreased carbon steel using a bar coater. The prepared coatings were then dried for 30 min at room temperature, followed by an additional 40 minutes at 80 °C. For comparative purposes, a reference coating (pure polyurethane coating) was prepared using a similar procedure as the experimental coatings.

Corrosion measurements were carried out in a conventional three-electrode cell enclosed within a Faraday cage. The configuration comprised a platinum counter electrode, a saturated calomel electrode (SCE) serving as the reference, and AISI 1080/1010 carbon steel functioning as the working electrode. Electrochemical impedance spectroscopy (EIS) measurements were conducted using a Gamry FAS2 Femtostat with a PCI4 Controller. Impedance spectra were recorded across a frequency range from  $1 \times 10^5$  Hz to  $1 \times 10^{-2}$  Hz, employing applying a sinusoidal amplitude (RMS) of 10 mV and 7 points



per decade, with respect to the open circuit potential. EIS measurements were employed to evaluate the corrosion resistance of the developed samples on carbon steel immersed in a 0.05 M NaCl aqueous solution. The deliberate selection of a 0.05 M NaCl electrolyte concentration was intended to induce the degradation of coated steel, allowing a comparison with the systematic inhibitive effect of LDHs/PU coatings over a 21-day period. For the understanding of active protection, EIS measurements were further studied on the artificial cross-scratched (3.5  $\mu\text{m}$  wide  $\times$  1.2 cm long) BTA and LDH-BTA base PU coatings on the coated carbon steels where the composite coatings were immersed in 0.05 M NaCl solution.

### 2.3. Environmental behavior of nanomaterials in aqueous dispersions over time

**2.3.1. Stability and size.** The behavior of Mg–Al LDH–BTA and Zn–Al LDH–BTA was evaluated in low and high ionic strength media, namely ultra-pure water (UPW; MilliQ®) and artificial saltwater (ASW; salinity of 35, prepared with Tropic Marin® Pro Reef salt; filtered through a 0.45  $\mu\text{m}$  cellulose acetate filter from PRAT DUMAS®). Dynamic light scattering (DLS) and zeta potential ( $\zeta_p$ ) measurements were performed daily (from 0 to 96 h) in aqueous dispersions with concentrations of 1.23 and 100  $\text{mg L}^{-1}$ , mimicking the conditions of the ecotoxicity testing ( $n = 3$ ). DLS was carried out using UPW and ASW, while zeta potential was performed only in UPW due to the characteristics of the sample cell cuvette.

**2.3.2. Metals dissolution and anionic release.** The concentrations of metals (zinc, magnesium, and aluminum) and anions (nitrates and chlorides; BTA was not quantified due to technical constraints) released into the media through the dissolution of nanomaterials and anionic exchange was performed in dispersions of the nanomaterials directly in ASW at the concentrations of 1.23, 11.1, and 100  $\text{mg L}^{-1}$ . These concentrations correspond to the lowest, intermediate, and highest tested concentrations in most exposure tests (*cf.* next chapter). All dispersions were prepared using artificial saltwater as described in sub-section 2.3.1. The stock solutions (100  $\text{mg L}^{-1}$ ) were placed in an ultrasonic bath for 30 minutes immediately after preparation. Then, the dispersions were maintained under the same conditions as most of the ecotoxicological assays (at the temperature of  $19 \pm 1$  °C and photoperiod of 16 h light: 8 h dark). At each timepoint (0, 24, 48, 72, and 96 h), two samples were collected: 15 mL for metal analysis, and 50 mL for anions analysis. All samples were centrifuged at 5000 rpm for 5 minutes (to ensure the nanoclays sedimentation and interrupt the physicochemical reactions after sampling). The supernatant was collected and stored at  $-20$  °C for the anions quantification; acidified with 2% nitric acid, and preserved at 4 °C for metal analysis.

Target metals were quantified using the inductively coupled plasma optical emission spectrometry (ICP-OES; HORIBA Jobin-Yvon, model Ultima). Detection limits were 0.01, 0.02, and 0.001  $\text{mg L}^{-1}$  for Al, Zn, and Mg, respectively.

Selected anions were determined through high-performance liquid chromatography (HPLC; Dionex, model ICS3000). Nitrate and nitrite were diluted 20-fold due to chloride content. Detection limits were 0.22 and 0.80  $\text{mg L}^{-1}$  for nitrate, and chlorides, respectively. Both analyses were conducted at the NOVA Lisbon University at the LAQV-REQUIMTE certified facilities (Caparica, Portugal).

### 2.4. Ecotoxicity testing

Several marine species were used to assess the effects of BTA, Mg–Al LDH–BTA and Zn–Al LDH–BTA. Acute tests were performed with the bacteria *Aliivibrio fischeri*, *Idiomarina seosinensis* and *Halobacillus locisalis*, the rotifer *Brachionus plicatilis*, the gastropods *Phorcus lineatus* and *Steromphala umbilicalis*, the bivalves *Scrobicularia plana*, *Mytilus galloprovincialis* and *Ruditapes philippinarum*, and the crustacean *Artemia salina*. Short-term chronic tests were performed with the microalgae *Isochrysis galbana* and *Tetraselmis chuii*, the diatoms *Phaeodactylum tricornutum* and *Chaetoceros calcitrans*, and the echinoderm *Paracentrotus lividus*. Ecotoxicity tests were classified as acute or short-term chronic based on duration, organism life cycles, specificity, biological effects, and guidance from standard protocols and literature.<sup>51–53</sup> Although microalgae growth inhibition tests follow acute testing timelines, ASTM considers them short-term chronic due to their ability to assess impacts over several generations, given microalgae's rapid life cycle.<sup>54</sup> Similarly, the echinoderm embryo development test, despite its brief duration, targets sensitive life stages and includes a sublethal endpoint, meeting EPA criteria for short-term chronic classification.<sup>55</sup>

The freeze-dried bacteria *A. fischeri* was prepared by rehydration with 1 mL of reconstitution solution and stored in the Microtox® analyzer at 4 °C, according to the manufacturer. The cultures of *I. seosinensis* and *H. locisalis* were made using agar (standard methods agar) and the artificial marine salt Tropic Marin® Pro Reef. Additionally, the culture of *H. locisalis* was supplemented with LB “broth (Miller)” medium. The cultures of microalgae and diatoms were prepared by adding 10 mL of Optimumedium (Aqualgae S.L.®) to 1 L of sterile filtered artificial saltwater (ASW; salinity ( $S$ ) = 35, 0.45  $\mu\text{m}$  pore size, cellulose acetate Prat Dumas® filters, and autoclaved 20 min at 120 °C). They were maintained at room temperature of  $19 \pm 1$  °C and photoperiod conditions of 16:8 h (light:dark). Microinvertebrates *B. plicatilis* and *A. salina* were hatched in the laboratory using ASW (salinity 20 and 25, respectively) at  $25 \pm 1$  °C under continuous light. Macroinvertebrates *P. lineatus*, *S. umbilicalis*, *M. galloprovincialis*, and *R. philippinarum* were collected in the intertidal rocky shore at Costa Nova (Canal de Mira, Portugal); *S. plana* in the intertidal muddy sandflats at Barra (Canal de Mira, Portugal) and *P. lividus* adults were collected at Buarcos (Portugal; 40°10'13.4"N 8°53'27.0"W). After field collection, animals were acclimated to laboratory conditions for 48 hours, using ASW ( $S = 35$ ) with continuous aeration, at constant room temperature of  $19 \pm 1$  °C, 16:8 h



light:dark photoperiod and no food provided (except for *P. lividus*, which were fed *ad libitum* with *Ulva* sp.). Gametes of *P. lividus* were obtained by inducing spawning by injecting 0.5–1.5 mL of 0.5 M KCl into the coelomic cavity of the organisms. After spawning, the gametes of five males and five females were mixed in sterile and filtered ASW ( $S = 35$ ). Using an optical microscope, egg fertilization success was verified, and the number of eggs was adjusted to a ratio of ~200 eggs per 0.05 mL.

Exposure tests were carried out in ASW (salinity 35; filtered at 0.45  $\mu\text{m}$ ; autoclaved at 120 °C for 20 min in the case of microalgae, rotifers, crustaceans and echinoderms) at a constant temperature of  $19 \pm 1$  °C and light:dark photoperiod of 16:8 h, with some exceptions: *A. fischeri* was supplied frozen and the Microtox® test conditions followed, while *B. plicatilis* and *Artemia salina* were kept at a constant temperature of  $25 \pm 1$  °C and in the dark. No medium renewal was performed during each exposure testing.

The exposure concentrations and experimental design details were defined according to each tested species and can be consulted in Table S1.† The lowest concentration tested was 0.393 mg L<sup>-1</sup> and the highest concentration was 100 mg L<sup>-1</sup>. In all cases, a negative control was included (ASW only). For Mg–Al LDH–BTA and Zn–Al LDH–BTA, the concentrations are expressed as mg of BTA per liter. The loading content of BTA is 20% and 25% of the total weight for Mg–Al LDH–BTA and Zn–Al LDH–BTA, respectively. Both nanomaterials contain 5% of Al and 28% of Zn or Mg, depending on the nanoforms. Values of pH, dissolved oxygen and temperature were monitored daily for macroinvertebrates.

**2.4.1. Statistical analysis.** One-way analysis of variance (one-way ANOVA) tests were conducted using GraphPad Prism v.9.0 to assess significant differences between treatments and control ( $p < 0.05$ ). NOEC (no observed effect concentration) and LOEC (lowest observed effect concentration) values were derived from these tests. This software was also used to compute L/E/IC<sub>50</sub> (*i.e.*, concentrations causing 50% mortality, effects or inhibition) *via* non-linear regression. Based on the derived L/I/EC<sub>50</sub> values, the toxicity of each compound was categorized as follows: extremely toxic (L/I/EC<sub>50</sub> < 0.1 mg L<sup>-1</sup>), very toxic (0.1–1 mg L<sup>-1</sup>), toxic (1–10 mg L<sup>-1</sup>), harmful (10–100 mg L<sup>-1</sup>) and non-toxic (L/I/EC<sub>50</sub> > 100 mg L<sup>-1</sup>), as explained by Figueiredo *et al.*<sup>56</sup> Additionally, these findings were aligned with current European legislation.

## 2.5. Hazard assessment

**2.5.1. Data selection.** The NOEC values acquired in this study were used to develop species sensitivity distributions and to determine the HC<sub>5</sub> and PNEC values for each compound. For BTA, additional data for the diatom *Skeletonema costatum* was obtained from the literature (NOEC value = 6.71 mg L<sup>-1</sup>).<sup>57</sup>

**2.5.2. Statistic PNEC determination.** The software ETX 2.3.1 was used to estimate the hazardous concentration at 5% (HC<sub>5</sub>) through species sensitivity distributions (SSDs) from a log-normal distribution. SSDs were constructed using

NOEC data. Data normality was assessed using the Anderson–Darling test ( $p < 0.05$ ), the Kolmogorov–Smirnov test ( $p < 0.05$ ) and the Cramer von Mises test ( $p < 0.05$ ). PNEC values were calculated by the ratio between HC<sub>5</sub> and an assessment factor of 5 (the most conservative factor), following the technical guidance document,<sup>58</sup> due to the use of acute and short-term chronic data.

In cases where several values for the same species were present, the geometric mean of the values was calculated. In the few situations where the NOEC value was lower than the lowest tested concentration, it was decided to use the LOEC value divided by an assessment factor of 10 (*i.e.*, in the case of the LDH–XX, the NOEC was lower than the lowest tested concentration (LOEC = 0.41 mg L<sup>-1</sup>) for the echinoderm *Paracentrotus lividus*, so the value considered in the SSD was 0.041 mg L<sup>-1</sup>). This strategy was a commitment to calculate the PNEC with a more conservative approach without ignoring or omitting the given absence for that species and chemical.

**2.5.3. Deterministic PNEC determination.** The deterministic PNEC was established using the lowest NOEC values within the dataset for each test compound. For all compounds, the lowest NOEC was then divided by an assessment factor (AF) of 1000 to obtain PNEC. This AF was chosen accordingly to REACH and the technical guidance document (*i.e.*, the dataset for all compounds contains short-term data for at least three taxonomic groups of three trophic levels, plus additional marine taxonomic groups).<sup>58</sup>

## 3. Results and discussion

Corrosion significantly impacts the marine industry by deteriorating metal structures, leading to substantial economic losses, and posing risk to the environment and humans.<sup>2,59</sup> One of the most common approaches to address these challenges involves integrating corrosion inhibitors into coatings applied to metallic surfaces.<sup>13,14,38</sup> However, the undesired interactions of the currently used corrosion inhibitors with other coating components, their high toxicity towards marine species and their uncontrolled and preliminary release into the environment, stress the necessity of identifying eco-friendlier and effective alternatives to replace the current inhibitors, together with a technology capable of reducing the leaching rate of these active substances.<sup>24,60,61</sup> Benzotriazole (BTA) is one of the most promising effective corrosion inhibitors, however it still poses concern regarding its toxicity.<sup>62</sup> Therefore, recent studies have reported that immobilizing corrosion inhibitors in ENMs, like layered-double hydroxides (LDHs), is a promising approach to reduce their toxicity and also mitigate their premature release, contributing to extending the duration of the corrosion protection.<sup>13,25,37,38</sup> This makes LDHs a promisor class of materials for creating a new generation of nanostructured pigments for marine coatings that are both environmentally safe and highly efficient. Therefore, the present study aimed at assessing the environmental behavior,



effects, and hazard of BTA in both soluble and nanostructured forms.

### 3.1. Characterization of engineered nanomaterials

**3.1.1. Physical and chemical properties.** LDH materials, obtained by co-precipitation process, followed by hydrothermal treatment (LDH-NO<sub>3</sub>) and anionic-exchange (LDH-BTA), were characterized regarding morphological, structural, and chemical properties. Fig. 2 shows the scanning electron microscope images of Zn-Al LDH-BTA and Mg-Al LDH-BTA. Both images demonstrate the agglomerated LDHs with the traditional clay-type morphology of such 2D nanomaterials. During the drying step, these types of nanomaterials tend to agglomerate, making it difficult to observe them in their individual state, as reported elsewhere.<sup>25</sup> Typically, such nanoclays have a platelet and hexagonal shape with a height of 20 to 40 nm and a length of large hundreds of nm.<sup>13,25,46</sup>

Regarding their structural analysis, XRD diffractograms of Mg-Al LDH-BTA and Zn-Al LDH-BTA are shown in Fig. 3. Concerning the LDH phases of Mg-Al LDH-BTA materials, prepared by anion exchange reactions of the LDH-nitrate parent composition, the diffraction reflections of the (00 $l$ ) family were shifted to lower angles, which indicates an increase in the basal spacing (BS) value in consequence to the larger size of BTA<sup>−</sup> regarding the parent nitrate anion. In this case, the gallery height was estimated to be 1.38 nm. With regards to Zn-Al LDH-BTA, the diffraction pattern suggests something different than the typical shift to lower two theta angles. In this case, a group of new phases is observed, both at higher and at lower two theta angles, suggesting the presence of some intercalated BTA but also a well-defined reflection, corresponding to a LDH phase with the basal spacing value of about 0.75 nm, characteristic of Zn-Al LDH intercalated with OH<sup>−</sup>. In agreement with previously published results,<sup>50</sup> the presence of unidentified phases suggests interactions between the Zn-Al hydroxide layers and BTA, with possible formation of phases based on zinc oxide/hydroxide and BTA and the substitution of nitrate by another anion.

Fig. 4 depicts the FT-IR spectra of the prepared materials. The analysis of the results shows common peaks to all, namely a broad band around 3400 cm<sup>−1</sup>, corresponding to stretching vibrations of the −OH groups of both layer hydroxide moieties and interlayer water, at 1000–600 cm<sup>−1</sup> assigned to the metal-hydroxide link (M–OH) and at 600–400 cm<sup>−1</sup> to the metal-oxygen link stretching vibrations (M–O), and at around 1650 cm<sup>−1</sup> another band due to the deformation vibration mode of OH bonds in water molecules. The presence of BTA was confirmed by the presence of several peaks in the 900–1300 cm<sup>−1</sup> region attributed to the C–N, N–N and N–H stretching vibration modes of the triazole group. Additionally, the presence of a broad band of *ca.* 1362 cm<sup>−1</sup> could be attributed to the presence of carbonate ions in these materials. Both Mg-Al LDH-BTA and Zn-Al LDH-BTA materials have BTA on its composition, confirming the success of its immobilization. In the next step, one of these materials was selected to show their application as anticorrosive pigment when incorporated into a coating matrix.

**3.1.2. Application as anticorrosive pigment.** Aiming to show the application of these materials as anticorrosive pigments, Zn-Al LDH-BTA was incorporated into a PU coating, applied on carbon steel substrates and studied using electrochemical techniques. The EIS study was conducted on Zn-Al LDH-BTA-based system, according to the ecotoxicological findings (as presented and discussed in the next section). This indicates that immobilizing BTA on Zn-Al-LDH, despite some challenges with BTA intercalation, can be an effective strategy for enhancing corrosion resistance properties when compared to the direct dispersion of BTA polyurethane. In fact, the protective effect of the coating on the steel substrate is clear, and the impedance values obtained for the coating systems are two to three orders of magnitude higher for the coated systems when compared to the bare carbon steel.

Among the coating systems prepared for short-term immersion (1 h), the impedance is the largest for the coating without BTA and LDH-BTA. The reason for this is well reported in the literature and is associated with disruption of

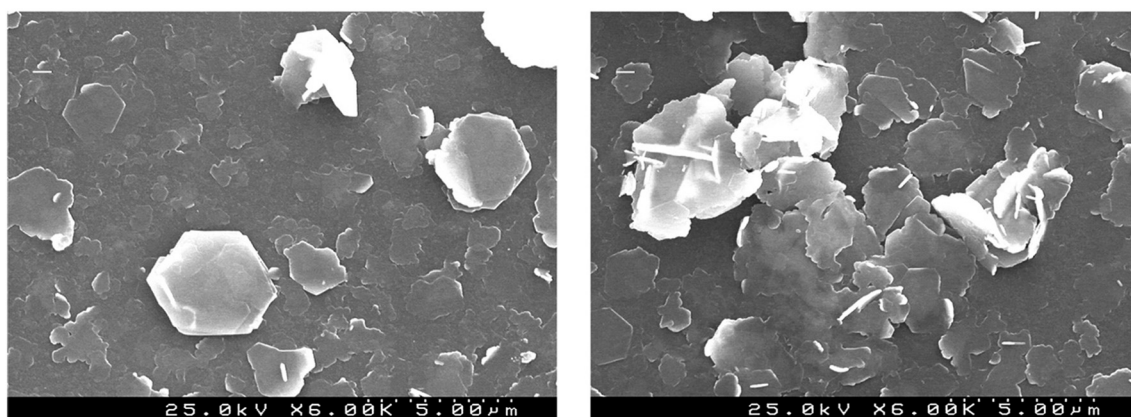


Fig. 2 SEM images of Mg-Al LDH-BTA (left) and Zn-Al LDH-BTA (right).



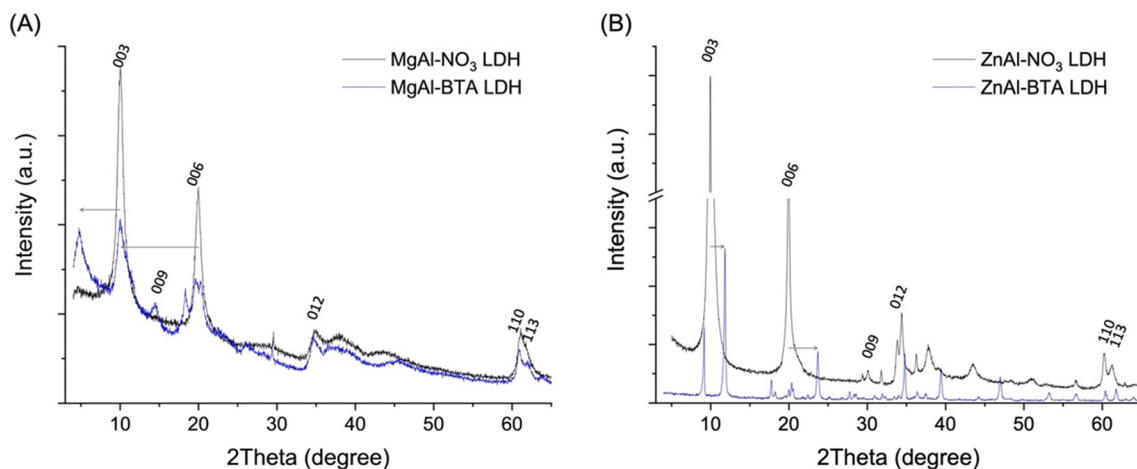


Fig. 3 XRD patterns of (A) Mg-Al LDH-BTA and (B) Zn-Al LDH-BTA.

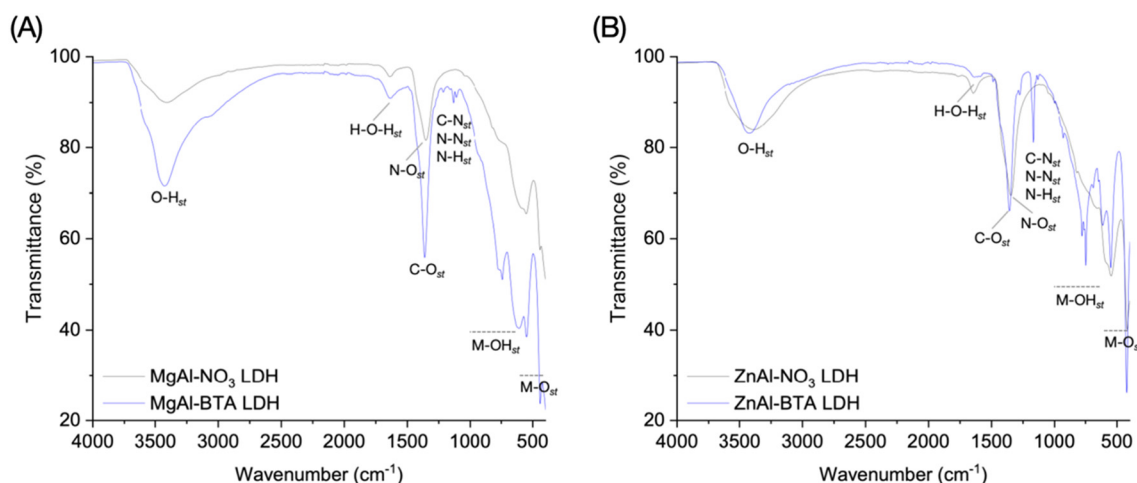


Fig. 4 Fourier transform infrared spectroscopy (FT-IR) spectra of (A) Mg-Al LDH-BTA (A) and (B) Zn-Al LDH-BTA.

the barrier properties of the coating when new additives are added, which may lead to local inhomogeneities due to inefficient dispersion of the LDH particles and/or detrimental interaction of BTA with coating matrix.<sup>63</sup> After an hour of immersion, the coating with BTA exhibited low-frequency impedance  $|Z|_{0.01\text{Hz}}$  of  $4 \times 10^5 \Omega\text{cm}^2$  (Fig. 5a) whereas LDH-BTA loaded coating showed  $|Z|_{0.01\text{Hz}}$  value of  $8 \times 10^5 \Omega\text{cm}^2$  (Fig. 5c). The reference PU coating has higher impedance values ( $|Z|_{0.01\text{Hz}}$  of  $2 \times 10^6 \Omega\text{cm}^2$ ). However, the ingress of electrolyte species over time through coating pores and microcracks is unstoppable. In the absence of particles that may increase tortuosity and increase the diffusion path length, such as LDHs, the barrier properties continuously decrease, becoming the least protective coating after 480 h of immersion. The BTA-loaded coating, on the other hand, exhibits the lowest impedance for early immersion stages, which is associated with detrimental interaction between the molecule and the binder.<sup>63</sup> Nevertheless, for longer immersion times the decay in the impedance is not as significant as for the reference coating, which may be due to

some protective effect rendered by BTA acting at the metal interface. The best coating system for long-immersion times is the coating loaded with LDH-BTA (Fig. 5c and d), which may be due to a combination of the positive contribution of LDH platelets for the barrier properties and the controlled release of BTA that acts on the metal/coating interface to reduce the corrosion rate when the electrolyte reaches the interface.

Fig. 6 shows the variation of  $|Z|_{0.01\text{Hz}}$   $\Omega\text{cm}^2$  during the whole monitored time (20 days), where it is clear to see that after 168 h of immersion, the best-performing system is the LDH-BTA coating. After 480 h, the  $|Z|_{0.01\text{Hz}}$  value of Zn-Al LDH-BTA/PU is  $5 \times 10^4 \Omega\text{cm}^2$ , compared to  $3 \times 10^3 \Omega\text{cm}^2$  for BTA/PU system and  $1 \times 10^3 \Omega\text{cm}^2$  for PU. Therefore, the incorporation of Zn-Al LDH-BTA in polyurethane coatings, demonstrates effectiveness in protecting steel structures against corrosion, with advantages such as a reduced impedance declining rate after 20 days and improved post-corrosion adhesion. These observed results are consistent with findings reported in other studies.<sup>47,49,64</sup>



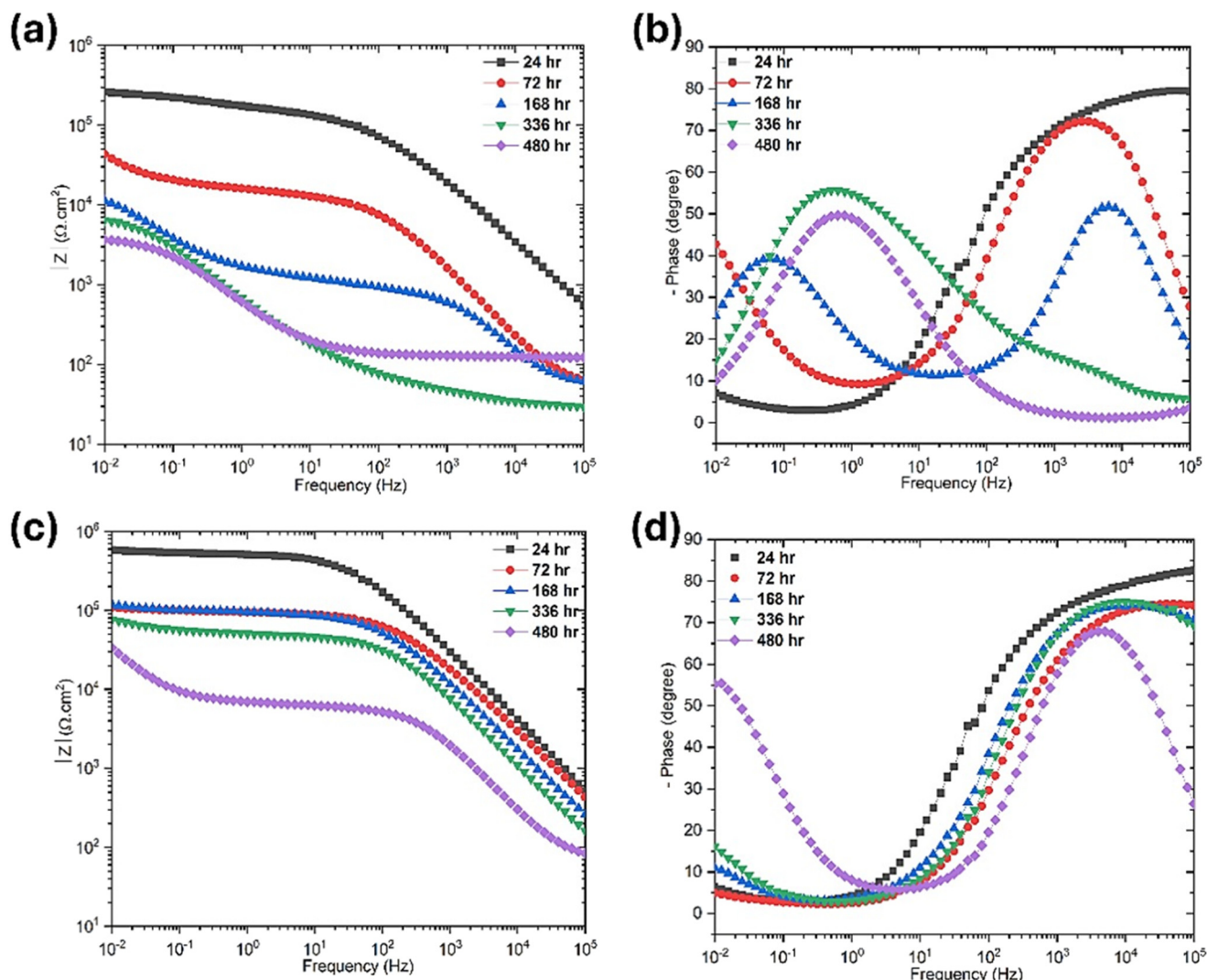


Fig. 5 Electrochemical impedance spectroscopy (EIS) spectra of polyurethane coating systems modified with benzotriazole in the soluble form (BTA; a and b) and nanostructured form (Zn-Al LDH-BTA; c and d) immersed in a 0.05 M NaCl aqueous solution over time (up to 480 h).

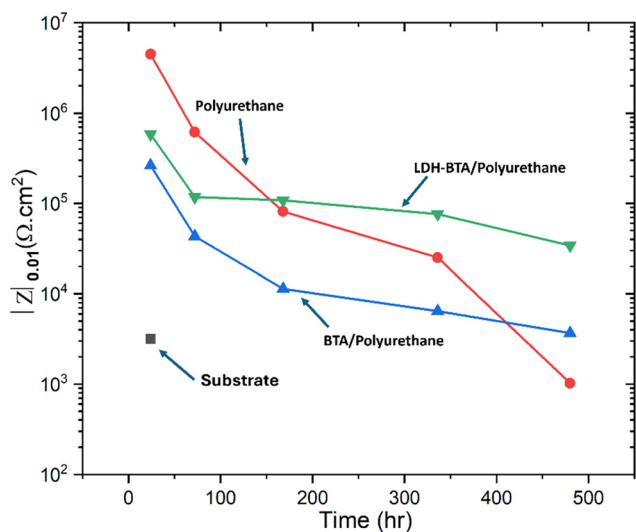


Fig. 6 Impedance modulus of studied surfaces at 0.01 Hz against various immersion times.

### 3.2. Behavior of nanomaterials in low and high ionic strength media

Fig. 7 presents the environmental behavior of Mg-Al LDH-BTA and Zn-Al LDH-BTA in low (UPW) and high (ASW) ionic strength media over time, based on particle size (A, C) and zeta potential values (B, D), respectively.

Zeta potential values measured in UPW exhibit concentration-dependent behavior. Additionally, the dispersions are generally unstable over time ( $30 \text{ mV} > \zeta\text{-potential} > -30 \text{ mV}$ ) in low ionic strength media. For Mg-Al LDH-BTA, the zeta potential remains approximately +15 mV over time at the lowest tested concentration, increasing to around +30 mV at  $100 \text{ mg L}^{-1}$ . In case of Zn-Al LDH-BTA, the zeta potential shifts from a negative value ( $\sim -25 \text{ mV}$ ) in the lowest concentration to a positive value ( $\sim +45 \text{ mV}$ ) at the highest tested concentration. It is known that the charge density of LDHs can be modified by adjusting the composition of metal cations within their structure.<sup>63</sup> In this case, the Zn-Al LDH version presented



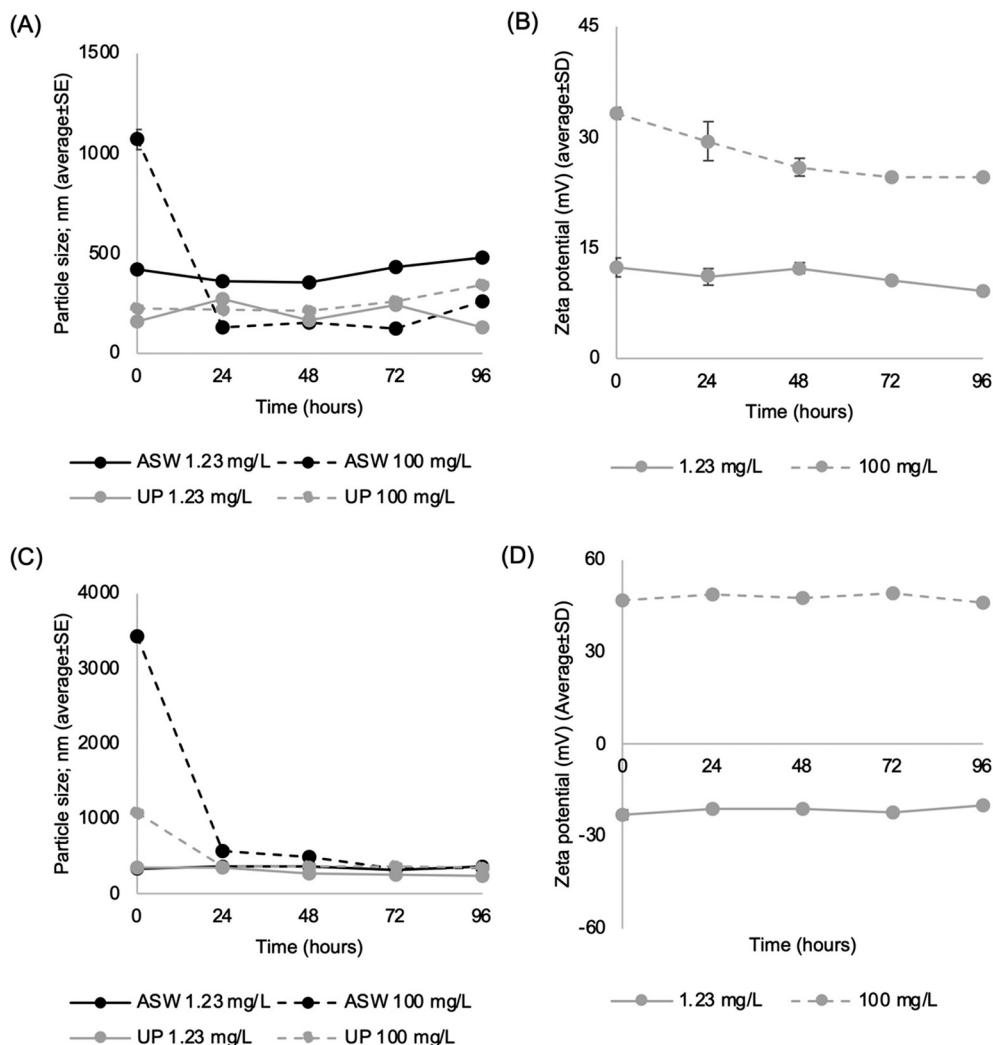


**Fig. 7** Effects of concentration and time on the zeta ( $\zeta$ ) potential and particles size of the colloidal dispersions of the anticorrosion nanomaterial Mg-Al LDH-BTA (A and B) and Zn-Al LDH-BTA (C and D) dispersed in ultra-pure water and artificial saltwater, respectively. Dots represent mean values and bars the standard error (SE) for particle size and standard deviation (SD) for zeta potential.

higher zeta potential values comparing to the Mg-Al LDH, which is in line with other studies.<sup>65,66</sup> However, this variation may also be attributed to a non-homogenous dissolution or to the desorption of BTA, which exposes the positively charged hydroxide layers, thereby affecting the zeta potential, particularly in the case of Zn-Al LDH-BTA.

Dynamic light scattering reveals that dispersions exhibit a high polydispersity index ( $PdI > 0.7$ ) in high ionic strength media and do not meet the criteria for optimal quality. This underscores the heterogeneity in particle size within suspensions, suggesting the potential presence of large aggregates/agglomerates. As a result, the particle size data relies on the average value ( $n = 3$ ) of the peak particle scattering intensity. Based on this data, it is possible to conclude that both Mg-Al LDH-BTA and Zn-Al LDH-BTA colloidal dispersions are unstable in aqueous solutions (artificial saltwater and ultra-pure water) and tend to form aggregates, especially at higher concentrations ( $100 \text{ mg L}^{-1}$ ). This tendency can be attributed to the decreased spacing between particles in denser dispersions,

which can promote aggregation and/or agglomeration processes. On the other hand, in the lowest concentration, it was observed that the particle size of LDH dispersions is more stable in UPW compared to ASW, over time. This occurs due to a decrease in the Debye length in media with higher ionic strength (such as ASW) which works as a shield, reducing electrostatic repulsion and allowing particles to be closer, which can also explain the larger particle size observed in LDHs dispersed in ASW.<sup>67</sup> Nonetheless, over time, the particle size tends to decrease and stabilize, which can be attributed to the sedimentation of larger particles at 0 h making them undetected by DLS, a tendency also reported for other nanomaterials. Such sedimentation behavior in nanomaterials may also influence zeta potential measurements<sup>68</sup> since particles with different zeta potential are left behind, potentially explaining the observed variations in zeta potential from the lowest to the highest tested concentrations.

Although these ENMs are unstable and prone to aggregation when directly dispersed in UPW or ASW, their real-life



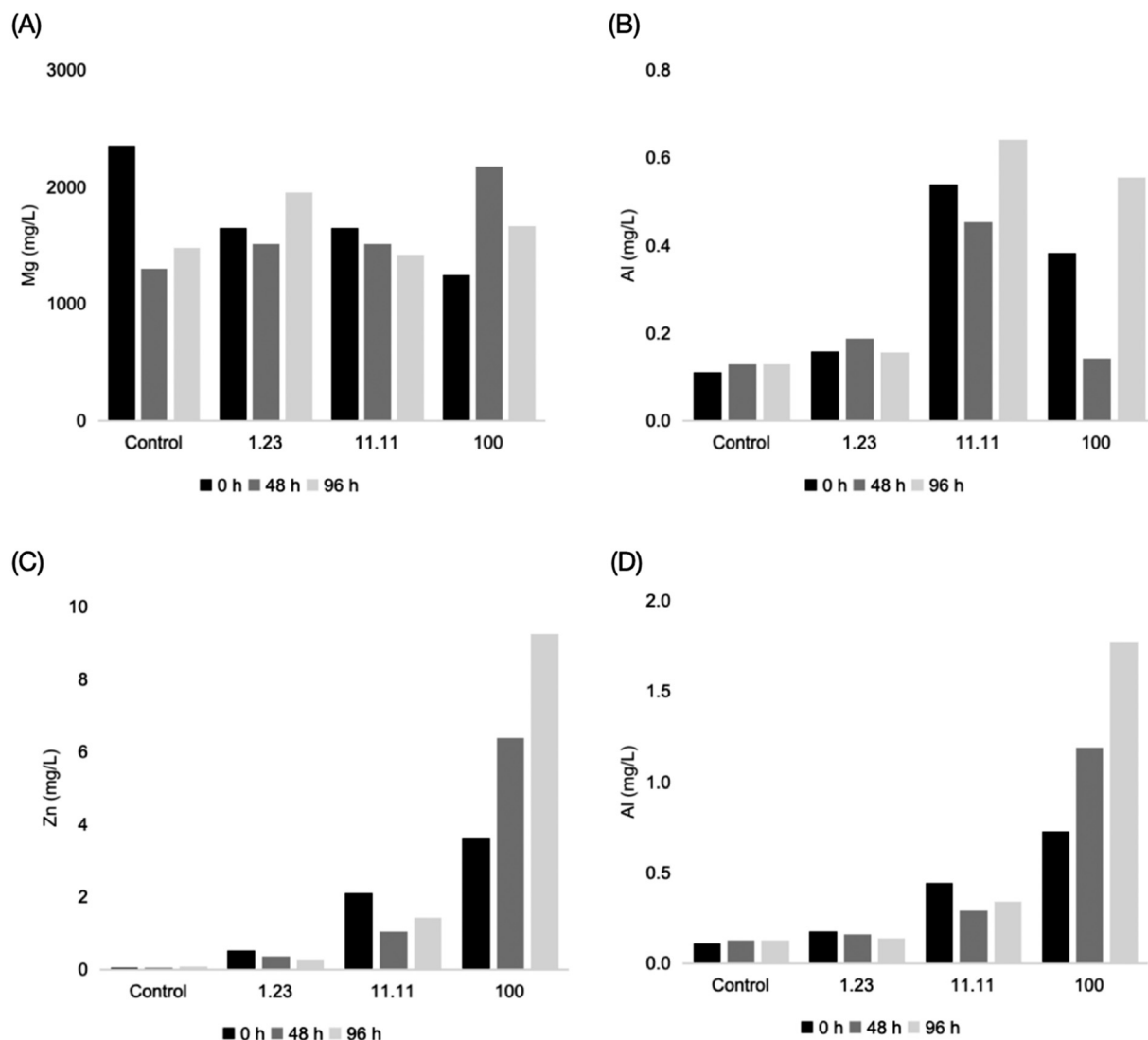


Fig. 8 Quantification of magnesium (Mg) and aluminum (Al) in aqueous dispersions of Mg-Al LDH-BTA (A and B) and of zinc (Zn) and aluminum (Al) in aqueous dispersions of Zn-Al LDH-BTA (C and D) over time. Dispersions were prepared in artificial saltwater at concentrations of 1.23, 11.11, and 100 mg BTA per L and in non-contaminated artificial seawater (negative control; *i.e.*, 0 mg BTA per L) ( $n = 1$ ).

applications will involve incorporation into polymeric coatings as additives. As such, ENMs are not expected to be present in the environment in their free form except in the event of an accidental spill. Under typical conditions, only a limited release of cations and anions from the ENMs is expected, with the release of intact ENMs occurring primarily through degradation or wear of the coating matrix. This would result in very low local concentrations of free ENMs, reducing the likelihood of homoaggregation while increasing the potential for heteroaggregation with other particles present in the environment, such as micro- and nanoplastics or natural colloids/sediments as demonstrated by other studies.<sup>69,70</sup>

### 3.3. Quantification of metals and anions on ENMs dispersions over time

Fig. 8 shows the quantification of magnesium, zinc, and aluminum of the dispersions of the engineered nanomaterials

Mg-Al LDH-BTA and Zn-Al LDH-BTA over time (Table S2† includes data for all timepoints).

Concerning dissolved magnesium in Mg-Al LDH-BTA dispersions, no particular time or concentration-dependent pattern was observed in opposition to aluminum that increases with the concentration of the dispersion and time, reaching a maximum of 0.64 mg Al per L (at 96 h in the concentration of 11.11 mg L<sup>-1</sup>). The control and the lowest tested concentration samples present a similar aluminum content over time.

Regarding Zn-Al LDH-BTA, the concentration of dissolved zinc and aluminum is consistently higher in the dispersions of 11.11 and 100 mg L<sup>-1</sup> across all timepoints compared to the control and the lowest tested concentration. The highest dissolved metal concentrations were 1.78 mg Al per L and 9.27 mg Zn per L for the dispersion of 100 mg L<sup>-1</sup> of the nanomaterial at the timepoint of 96 h.



**Table 1** Toxicity of BTA towards a total of 10 marine species, expressed as the NOEC (no observed effect concentration) and median lethal, inhibition or effect concentration (L/E/IC<sub>50</sub>) values. L/E/IC<sub>50</sub> data was used to categorize the toxicity of this compound following the EC Directive 93/67/EEC classification scheme, adapted by Blaise et al.<sup>81</sup> for ENMs: extremely toxic (L/E/IC<sub>50</sub> < 0.1 mg L<sup>-1</sup>), very toxic (L/E/IC<sub>50</sub> = 0.1–1 mg L<sup>-1</sup>), toxic (L/E/IC<sub>50</sub> = 1–10 mg L<sup>-1</sup>), harmful (L/E/IC<sub>50</sub> = 10–100 mg L<sup>-1</sup>) and not toxic (L/E/IC<sub>50</sub> > 100 mg L<sup>-1</sup>). 95% CI – confidence interval at 95%. n.a. – not applicable

Phylum	Species	Endpoint	Exposure type	NOEC	LOEC	L/E/IC <sub>50</sub>	95% CI	Toxicity
Proteobacteria	<i>Aliivibrio fischeri</i>	Luminescence inhibition (15 min)	Acute	25	50	42.4	25.2–73.5	Harmful
Rotifera	<i>Brachionus plicatilis</i>	Lethality (48 h)	Chronic	100	>100	>100	n.a.	Not toxic
Mollusca	<i>Phorcus lineatus</i>	Lethality (96 h)		100	>100	>100	n.a.	Not toxic
	<i>Ruditapes philippinarum</i>	Lethality (96 h)		100	>100	>100	n.a.	Not toxic
Arthropoda	<i>Artemia salina</i>	Lethality (48 h)		100	>100	>100	n.a.	Not toxic
Bacillariophyta	<i>Phaeodactylum tricornutum</i>	Growth inhibition (72 h)		3.7	11.11	>100	n.a.	Not toxic
Ochrophyta	<i>Chaetoceros calcitrans</i>	Growth inhibition (72 h)		100	>100	>100	n.a.	Not toxic
Chromista	<i>Isochrysis galbana</i>	Growth inhibition (72 h)		33.33	100	>100	n.a.	Not toxic
Chlorophyta	<i>Tetraselmis chuii</i>	Growth inhibition (72 h)		100	>100	>100	n.a.	Not toxic
Echinodermata	<i>Paracentrotus lividus</i>	Pluteus formation (48 h)		0.137	0.41	2.36	1.70–5.72	Toxic

In terms of anions analysis, Tables S3 and S4,<sup>†</sup> display the measured contents for Mg–Al LDH–BTA and Zn–Al LDH–BTA, respectively. Regarding chloride content, no pattern was observed for either engineered nanomaterials. Nitrate was detected in the highest concentration of Mg–Al LDH–BTA across all timepoints (with a peak of 67.5 mg NO<sub>3</sub><sup>-</sup> per L at 0 h), and at 0 and 96 h for Zn–Al LDH–BTA (with a peak of 5.32 mg NO<sub>3</sub><sup>-</sup> per L at 0 h), probably due to some residual nitrate from the LDH precursor (*i.e.* LDH–NO<sub>3</sub>) which was not fully replaced by BTA.

### 3.4. Ecotoxicity testing

The effects of BTA, Mg–Al LDH–BTA and Zn–Al LDH–BTA are presented in Tables 1–3, respectively. BTA exhibited detrimental effects on the bacteria *A. fischeri* (IC<sub>50</sub> = 42.4 mg L<sup>-1</sup>) and the echinoderm *P. lividus* (EC<sub>50</sub> = 2.36 mg L<sup>-1</sup>), being classified as harmful and toxic, respectively. Regarding LDHs, Mg–Al LDH–BTA was harmful to the bacteria *A. fischeri* (IC<sub>50</sub> = 89.5 mg BTA per L) and to the microalgae *I. galbana* (IC<sub>50</sub> = 62.2 mg BTA per L) and *T. chuii* (IC<sub>50</sub> = 85.2 mg BTA per L)

and toxic towards the echinoderm *P. lividus* (EC<sub>50</sub> = 3.23 mg BTA per L). Concerning Zn–Al LDH–BTA, this engineered nanomaterial only presented toxicity towards *P. lividus*, being considered as very toxic (EC<sub>50</sub> = 0.43 mg BTA per L). Additionally, for all tested compounds, the lowest NOEC was recorded for the echinoderm *P. lividus*. These findings may be linked to the release of metals and anions from the ENMs (see section 3.3), as evidenced by the observed release of nitrate, zinc, magnesium, and aluminum. In Mg–Al LDH–BTA, nitrate was consistently detected at the highest tested concentration (100 mg BTA per L), peaking at 67.50 mg NO<sub>3</sub><sup>-</sup> per L at 0 h (Table S3<sup>†</sup>). For Zn–Al LDH–BTA, detectable nitrate concentrations were only observed in the 100 mg BTA per L dispersion at 0 and 96 h (maximum of 5.32 mg NO<sub>3</sub><sup>-</sup> per L) (Table S4<sup>†</sup>). It has been reported that nitrate can induce toxic effects in marine organisms at a concentration of 20 mg L<sup>-1</sup>, which can explain the increased toxicity of Mg–Al LDH–BTA when compared to BTA and Zn–Al LDH–BTA.

On the other hand, the metals' release from the nanostructures to the aqueous dispersion suggests a partial

**Table 2** Toxicity of Mg–Al LDH–BTA towards a total of 15 marine species, expressed as the NOEC (no observed effect concentration) and median lethal, inhibition or effect concentration (L/E/IC<sub>50</sub>) values. L/E/IC<sub>50</sub> data was used to categorize the toxicity of this compound following the EC Directive 93/67/EEC classification scheme, adapted by Blaise et al. for ENMs: extremely toxic (L/E/IC<sub>50</sub> < 0.1 mg L<sup>-1</sup>), very toxic (L/E/IC<sub>50</sub> = 0.1–1 mg L<sup>-1</sup>), toxic (L/E/IC<sub>50</sub> = 1–10 mg L<sup>-1</sup>), harmful (L/E/IC<sub>50</sub> = 10–100 mg L<sup>-1</sup>) and not toxic (L/E/IC<sub>50</sub> > 100 mg L<sup>-1</sup>). 95% CI – confidence interval at 95%. n.a. – not applicable

Phylum	Species	Endpoint	Exposure type	NOEC	LOEC	L/E/IC <sub>50</sub>	95% CI	Toxicity
Proteobacteria	<i>Aliivibrio fischeri</i>	Luminescence inhibition (15 min)	Acute	25	50	89.5	69.6–127	Harmful
Pseudomonata	<i>Idiomarina seosinensis</i>	Growth inhibition (24 h)	Chronic	100	>100	>100	n.a.	Not toxic
Firmicutes	<i>Halobacillus locisalis</i>	Growth inhibition (24 h)		<1	1	>100	n.a.	Not toxic
Rotifera	<i>Brachionus plicatilis</i>	Lethality (48 h)		100	>100	>100	n.a.	Not toxic
Mollusca	<i>Phorcus lineatus</i>	Lethality (96 h)		100	>100	>100	n.a.	Not toxic
	<i>Steromphala umbilicalis</i>	Lethality (96 h)		100	>100	>100	n.a.	Not toxic
	<i>Scrobicularia plana</i>	Lethality (96 h)		100	>100	>100	n.a.	Not toxic
	<i>Mytillus galloprovincialis</i>	Lethality (96 h)		100	>100	>100	n.a.	Not toxic
	<i>Ruditapes philippinarum</i>	Lethality (96 h)		100	>100	>100	n.a.	Not toxic
Arthropoda	<i>Artemia salina</i>	Lethality (48 h)		100	>100	>100	n.a.	Not toxic
Bacillariophyta	<i>Phaeodactylum tricornutum</i>	Growth inhibition (72 h)		3.33	11.1	70.7	56.4–93.2	Harmful
Ochrophyta	<i>Chaetoceros calcitrans</i>	Growth inhibition (72 h)		100	>100	>100	n.a.	Not toxic
Chromista	<i>Isochrysis galbana</i>	Growth inhibition (72 h)		<1	1	62.2	6.21–118	Harmful
Chlorophyta	<i>Tetraselmis chuii</i>	Growth inhibition (72 h)		3.33	11.1	85.2	69.3–111	Harmful
Echinodermata	<i>Paracentrotus lividus</i>	Pluteus formation (48 h)		0.41	1.23	3.23	2.07–5.72	Toxic



**Table 3** Toxicity of Zn-Al LDH-BTA towards a total of 15 marine species, expressed as the NOEC (no observed effect concentration) and median lethal, inhibition or effect concentration (L/E/IC<sub>50</sub>) values. L/E/IC<sub>50</sub> data was used to categorize the toxicity of this compound following the EC Directive 93/67/EEC classification scheme, adapted by Blaise *et al.* for ENMs: extremely toxic (L/E/IC<sub>50</sub> < 0.1 mg L<sup>-1</sup>), very toxic (L/E/IC<sub>50</sub> = 0.1–1 mg L<sup>-1</sup>), toxic (L/E/IC<sub>50</sub> = 1–10 mg L<sup>-1</sup>), harmful (L/E/IC<sub>50</sub> = 10–100 mg L<sup>-1</sup>) and not toxic (L/E/IC<sub>50</sub> > 100 mg L<sup>-1</sup>). 95% CI – confidence interval at 95%. n.a. – not applicable. n.c. – not calculable

Phylum	Species	Endpoint	Exposure type	NOEC	LOEC	L/E/IC <sub>50</sub>	95% CI	Toxicity
Proteobacteria	<i>Aliivibrio fischeri</i>	Luminescence inhibition (15 min)	Acute	100	>100	>100	n.a.	Not toxic
Pseudomonata	<i>Idiomarina seosinensis</i>	Growth inhibition (24 h)		100	>100	>100	n.a.	Not toxic
Firmicutes	<i>Halobacillus locisalis</i>	Growth inhibition (24 h)		<1	1	>100	n.a.	Not toxic
Rotifera	<i>Brachionus plicatilis</i>	Lethality (48 h)		100	>100	>100	n.a.	Not toxic
Mollusca	<i>Phorcus lineatus</i>	Lethality (96 h)		100	>100	>100	n.a.	Not toxic
	<i>Steromphala umbilicalis</i>	Lethality (96 h)		100	>100	>100	n.a.	Not toxic
	<i>Scrobicularia plana</i>	Lethality (96 h)		100	>100	>100	n.a.	Not toxic
	<i>Mytilus galloprovincialis</i>	Lethality (96 h)		100	>100	>100	n.a.	Not toxic
	<i>Ruditapes philippinarum</i>	Lethality (96 h)		100	>100	>100	n.a.	Not toxic
	<i>Artemia salina</i>	Lethality (48 h)		100	>100	>100	n.a.	Not toxic
	<i>Phaeodactylum tricornutum</i>	Growth inhibition (72 h)	Chronic	100	>100	>100	n.a.	Not toxic
Bacillariophyta	<i>Chaetoceros calcitrans</i>	Growth inhibition (72 h)		100	>100	>100	n.a.	Not toxic
Ochrophyta	<i>Isochrysis galbana</i>	Growth inhibition (72 h)		100	>100	>100	n.a.	Not toxic
Chromista	<i>Tetraselmis chuii</i>	Growth inhibition (72 h)		100	>100	>100	n.a.	Not toxic
Chlorophyta	<i>Paracentrotus lividus</i>	Pluteus formation (48 h)		0.137	0.41	0.43	0.34–0.52	Very toxic

dissolution of the LDH,<sup>25,43,71</sup> which can also explain the observed toxicity on the tested marine species at high exposure concentrations. In the Mg-Al LDH-BTA dispersions, the maximum detected aluminum concentration was 0.64 mg Al per L, while in the Zn-Al LDH-BTA dispersions, the maximum concentrations of aluminum and zinc were 1.78 and 9.27 mg L<sup>-1</sup>, respectively (Fig. 8). Aluminum has been shown to cause embryotoxicity in mussels (with an EC<sub>10</sub> of 250 µg Al per L for *Mytilus edulis*)<sup>72</sup> and oysters (with an EC<sub>10</sub> of 410 µg Al per L for *Saccostrea echinata*).<sup>72</sup> It also leads to growth inhibition in various species of microalgae, such as *Tetraselmis* sp. (with an EC<sub>10</sub> of 250 µg Al per L)<sup>72</sup> and *Cylindrotheca closterium* (with an EC<sub>10</sub> of 80 µg Al per L).<sup>73</sup> Additionally, this metal can impair sea-urchin development when exposed to aluminum concentrations ranging from 2.7 to 2700 µg Al per L.<sup>74,75</sup> Therefore, given that the aluminum content released from the nanomaterials exceeds the concentrations known to induce toxicity in marine species, it may be a potential factor contributing to the observed toxicity, particularly with regard to Mg-Al LDH-BTA. In the case of Zn-Al LDH-BTA, together with the aluminum release, its toxicity towards the echinoderm *P. lividus* can also be linked to zinc release from the nanomaterial. This aligns with previous studies reporting that zinc can adversely affect the development of sea urchin embryos even at

low concentrations (96 h EC<sub>50</sub> = 0.23 mg Zn per L for *Strongylocentrotus droebachiensis* and *Strongylocentrotus purpuratus*).<sup>76</sup>

### 3.5. Hazard assessment

Fig. S1–S3† illustrate the species sensitivity distributions for the three tested compounds. The most sensitive species to all tested compounds was the echinoderm *Paracentrotus lividus*. Table 4 shows the hazardous concentrations at 5% and PNEC values of BTA, Mg-Al LDH-BTA and Zn-Al LDH-BTA. Despite that Mg-Al LDH-BTA demonstrated effects in terms of toxicity on more species (Table 2), the hazard assessment demonstrated that this nanomaterial had the highest statistical PNEC value, surpassing PNEC values for BTA and Zn-Al LDH-BTA by more than 2-fold. In terms of deterministic PNEC, Zn-Al LDH-BTA exhibited the highest value, being 3-fold higher than the PNEC values for the other two tested compounds. A comparison of both PNEC derivation approaches reveals that the deterministic approach allows to determine more conservative PNECs.

Moreover, these findings will be critical for regulatory purposes, specifically for the preparation of future REACH dossiers of both nanoforms and will complement the ECHA

**Table 4** Hazardous concentrations 5% (HC<sub>5</sub>) obtained from species sensitivity distributions using NOEC data for the different species and PNEC values. *n* is the sample size and tests for normality included: The Anderson–Darling test, the Kolmogorov–Smirnov test and the Cramer von Mises test. PNEC<sub>stat</sub> – statistic PNEC, derived from the HC<sub>5</sub> with AF = 5; PNEC<sub>determ</sub> – deterministic PNEC, derived from the lowest NOEC with AF = 1000 (according to TGD, 2003)

Contaminant	<i>n</i>	HC <sub>5</sub>	CI 95%	Normality tests	PNEC <sub>stat</sub>	PNEC <sub>determ</sub>
BTA	11	0.722	0.069–2.852	Rejected <sup>a</sup>	0.144	0.000137
Mg-Al LDH-BTA	15	1.628	0.276–5.076	Rejected	0.326	0.000137
Zn-Al LDH-BTA	15	0.619	0.096–2.055	Rejected	0.124	0.000410

<sup>a</sup> Only accepted in Kolmogorov–Smirnov test at the significance level of 0.01.



database for BTA. In fact, although BTA was not monitored in the present study due to technical limitations, it is likely that BTA also played a key role in the observed toxicity (in the soluble and both nanoforms) together with the other dissolved metals (as previously discussed). According to the classification criteria for substances outlined in the European Legislation, specifically by REACH, the soluble BTA and the two nanomaterials (Mg–Al LDH–BTA and Zn–Al LDH–BTA) fall into the “Chronic 2” category ( $\text{NOEC} \leq 1 \text{ mg L}^{-1}$ ). This categorization relies on the NOEC values for the echinoderm *Paracentrotus lividus*, which were 0.137 mg BTA per L for BTA and Zn–Al LDH–BTA and 0.41 mg BTA per L for Mg–Al LDH–BTA. This classification is designated for non-rapidly degradable substances having adequate chronic toxicity data available for one or two trophic levels, namely fish and/or crustacea and/or algae or other aquatic plants. Considering that echinoderms, specifically sea urchins, can be considered as secondary consumers, since they feed on plankton, kelp and algae, as well as prey on sea cucumbers, polychaetes, sponges, mussels, and barnacles,<sup>77</sup> the *P. lividus* embryotoxicity data were used as a replacement of the lack of fish embryotoxicity data. The large marine ecotoxicity dataset of BTA (presented herein) and the proposed classification reinforces the current classification of BTA as “toxic to aquatic life with long lasting effects” (provided by companies to ECHA),<sup>17</sup> supporting the claim that BTA is more eco-friendly than other state-of-the-art CIs, such as MBT, regarded as very toxic (acute and chronic).<sup>16,25</sup> Therefore, this study provides new scientific evidence for a future formal classification of BTA, approved by ECHA.

In summary, according to the current findings, both safe and sustainable by design (SSbD) nanomaterials demonstrate superior anti-corrosion and environmental performance, with the advantage of reducing the premature leaching of BTA from conventional coatings. The use of LDHs for immobilizing BTA represents a promising method for corrosion protection while decreasing its hazard, as evidenced by the lowest statistical and deterministic PNEC values for Mg–Al LDH–BTA and Zn–Al LDH–BTA, respectively. Additionally, LDHs are considered promising materials within a SSbD framework due to their relatively low environmental impact. LDHs are typically low to no toxic to marine and freshwater organisms<sup>25,42,43</sup> and their synthesis can often be achieved *via* low-energy, aqueous-based processes,<sup>78,79</sup> further enhancing their sustainability. Additionally, LDHs exhibit high anion exchange capacity and stability, allowing for controlled release or immobilization of functional additives,<sup>13,25,37,38,80</sup> which can reduce environmental emissions of the active ingredients over the product lifecycle. Their potential compatibility with bio-based or degradable polymeric matrices also contributes to circular material design. Overall, LDHs offer a resource-efficient and environmentally conscious alternative for functional additives. This underscores the importance of adopting a balanced approach that addresses both the technical demands of corrosion protection and environmental protection. Such an approach also aligns with the increasing recognition of sustainable and eco-friendly

practices across diverse industrial sectors, particularly the maritime coatings industry. Moreover, conducting additional research, especially focused on long-term exposure and sub-chronic effects, is essential to achieve a more thorough understanding and assessment of the potential hazards linked to these innovative anti-corrosion nanomaterials. Furthermore, in real-world applications, these nanomaterials will be incorporated into coatings, being not expected to be used in their free form. Thus, in the near future, it is crucial to test also the ecotoxicity and chemistry of coatings leachates, in addition to the pristine nanomaterials (the scope of the present study), to holistically assess and understand these nanoclays. When incorporated into coatings, the bioavailability of these nanomaterials – and intercalated active ingredients – is likely to be further diminished, and thus, the hazard of the developed nanostructured anti-corrosion pigment is expected to decrease even more, reinforcing the eco-friendly labeling herein proposed.

## 4. Conclusions

The present study provides the first holistic study in terms of the anti-corrosion efficacy, environmental behavior, ecotoxicity, and hazard of novel BTA-based nanomaterials, offering valuable insights that can be further supplemented for understanding and managing the environmental risks linked with these emerging nanomaterials. Overall, the novel nanomaterials demonstrated instability in aqueous solutions, showing tendencies to aggregate/agglomerate in low and high ionic strength media. Nevertheless, the incorporation of Zn–Al LDH–BTA in polyurethane coatings seems to improve corrosion protection when compared with reference coatings and coatings containing only the soluble form of BTA. Although the novel nanomaterials, particularly Mg–Al LDH–BTA, showed toxicity towards a higher number of species, immobilizing BTA in LDHs allowed for the reduction of its hazard towards marine species. Therefore, this approach appears to be a promising alternative for the development of more efficient corrosion inhibitors without compromising environmental safety. Further studies are imperative to assess the long-term, sub-cellular and bioaccumulation effects posed by these nanomaterials.

## Data availability

Data is openly available in Zenodo at <https://doi.org/10.5281/zenodo.12964404>.

## Conflicts of interest

There are no conflicts to declare.

## Acknowledgements

This work was developed in the scope of the NANOGREEN project “Towards a new generation of sustainable nano-based additives for maritime anti-corrosion smart coatings: a



multidisciplinary framework within the Atlantic" (CIRCNA/BRB/0291/2019; DOI: 10.54499/CIRCNA/BRB/0291/2019) funded by national funds (OE), through the Portuguese Foundation for Science and Technology, I.P. (FCT). Thanks are also due to FCT for the financial support through national funds to CESAM – Centre for Environmental and Marine Studies (UID/50006 + LA/P/0094/2020) and CICECO – Aveiro Institute of Materials (UIDB/50011/2020, UIDP/50011/2020 & LA/P/0006/2020). R. Martins was hired under the Scientific Employment Stimulus – Individual Call funded by national funds (OE), through FCT (2021.00386.CEECIND/CP1659/CT0011, DOI: 10.54499/2021.00386.CEECIND/CP1659/CT0011). J. Figueiredo and F. Perina were awarded with a grant (BI/UI88/8183/2023) and a researcher contract through the research project NANOGREEN (CIRCNA/BRB/0291/2019).

## References

- 1 P. Jain, B. Patidar and J. Bhawsar, Potential of Nanoparticles as a Corrosion Inhibitor: A Review, *J. Bio- Tribo-Corros.*, 2020, **6**(2), 43.
- 2 Z. Sabet-Bokati, K. Sabet-Bokati, Z. Russell, K. Morshed-Behbahani and S. Ouanani, Anticorrosion shape memory-assisted self-healing coatings: A review, *Prog. Org. Coat.*, 2024, **188**, 108193.
- 3 J. C. Kurth, P. D. Krauss and S. W. Foster, Corrosion Management of Maritime Infrastructure, *Transp. Res. Rec.*, 2019, **2673**(12), 2–14.
- 4 H. Kania, Corrosion and Anticorrosion of Alloys/Metals: The Important Global Issue, *Coatings*, 2023, **13**(2), 216.
- 5 R. Bender, D. Féron, D. Mills, S. Ritter, R. Bäßler and D. Bettge, *et al.*, Corrosion challenges towards a sustainable society, *Mater. Corros.*, 2022, **73**(11), 1730–1751.
- 6 B. Hou, X. Li, X. Ma, C. Du, D. Zhang and M. Zheng, *et al.*, The cost of corrosion in China, *npj Mater. Degrad.*, 2017, **1**(1), 4.
- 7 G. Koch, Cost of corrosion, in *Trends in Oil and Gas Corrosion Research and Technologies*, Elsevier, 2017, pp. 3–30.
- 8 U. M. Angst, A Critical Review of the Science and Engineering of Cathodic Protection of Steel in Soil and Concrete, *Corrosion*, 2019, **75**(12), 1420–1433.
- 9 S. A. Umoren and M. M. Solomon, Protective polymeric films for industrial substrates: A critical review on past and recent applications with conducting polymers and polymer composites/nanocomposites, *Prog. Mater. Sci.*, 2019, **104**, 380–450.
- 10 K. Tamalmani and H. Husin, Review on Corrosion Inhibitors for Oil and Gas Corrosion Issues, *Appl. Sci.*, 2020, **10**(10), 3389.
- 11 J. V. d. S. Araujo, M. Milagre and I. Costa, A historical, statistical and electrochemical approach on the effect of microstructure in the anodizing of Al alloys: a review, *Crit. Rev. Solid State Mater. Sci.*, 2023, 1–61.
- 12 P. A. Sørensen, S. Kiil, K. Dam-Johansen and C. E. Weinell, Anticorrosive coatings: A review, *J. Coat. Technol. Res.*, 2009, **6**(2), 135–176.
- 13 J. Tedim, S. K. Poznyak, A. Kuznetsova, D. Raps, T. Hack and M. L. Zheludkevich, *et al.*, Enhancement of active corrosion protection via combination of inhibitor-loaded nanocontainers, *ACS Appl. Mater. Interfaces*, 2010, **2**(5), 1528–1535.
- 14 C. Erdogan and G. Swain, Conceptual Sacrificial Anode Cathodic Protection Design for offshore wind monopiles, *Ocean Eng.*, 2021, **235**, 109339.
- 15 M. Rehioui, Controlling Corrosion Using Non-Toxic Corrosion Inhibitors, in *Introduction to Corrosion – Basics and Advances*, IntechOpen, 2023.
- 16 European Chemicals Agency (ECHA), <https://echa.europa.eu/pt/substance-information/-/substanceinfo/100.005.216>, Substance Infocard (Benzothiazole-2-thiol).
- 17 European Chemicals Agency (ECHA), <https://echa.europa.eu/pt/substance-information/-/substanceinfo/100.002.177>, Substance Infocard (Benzotriazole).
- 18 L. K. M. O. Goni and M. A. J. Mazumder, Green corrosion inhibitors, in *Corrosion inhibitors*, ed. A. Singh, 4th edn, 2019, pp. 77–83.
- 19 D. A. Leal, A. Kuznetsova, G. M. Silva, J. Tedim, F. Wypych and C. E. B. Marino, Layered materials as nanocontainers for active corrosion protection: A brief review, *Appl. Clay Sci.*, 2022, **225**, 106537.
- 20 E. Alibakhshi, E. Ghasemi, M. Mahdavian and B. Ramezanzadeh, A comparative study on corrosion inhibitive effect of nitrate and phosphate intercalated Zn-Al-layered double hydroxides (LDHs) nanocontainers incorporated into a hybrid silane layer and their effect on cathodic delamination of epoxy topcoat, *Corros. Sci.*, 2017, **115**, 159–174.
- 21 Z. Manoli, D. Pecko, G. Van Assche, J. Stiens, A. Pourkazemi and H. Terryn, Transport of Electrolyte in Organic Coatings on Metal, in *Paint and Coatings Industry*, IntechOpen, 2019.
- 22 M. F. Montemor, Functional and smart coatings for corrosion protection: A review of recent advances, *Surf. Coat. Technol.*, 2014, **258**, 17–37.
- 23 F. Zhang, P. Ju, M. Pan, D. Zhang, Y. Huang and G. Li, *et al.*, Self-healing mechanisms in smart protective coatings: A review, *Corros. Sci.*, 2018, **144**, 74–88.
- 24 K. Auepattana-Aumrung and D. Crespy, Self-healing and anticorrosion coatings based on responsive polymers with metal coordination bonds, *Chem. Eng. J.*, 2023, **452**, 139055.
- 25 R. Martins, T. Oliveira, C. Santos, A. Kuznetsova, V. Ferreira and F. Avelas, *et al.*, Effects of a novel anticorrosion engineered nanomaterial on the bivalve *Ruditapes philippinarum*, *Environ. Sci.: Nano*, 2017, **4**(5), 1064–1076.
- 26 A. Kuznetsova, P. M. Domingues, T. Silva, A. Almeida, M. L. Zheludkevich and J. Tedim, *et al.*, Antimicrobial activity of 2-mercaptobenzothiazole released from environmentally friendly nanostructured layered double hydroxides, *J. Appl. Microbiol.*, 2017, **122**(5), 1207–1218.
- 27 A. Nagiub and F. Mansfeld, Evaluation of corrosion inhibition of brass in chloride media using EIS and ENA, *Corros. Sci.*, 2001, **43**(11), 2147–2171.
- 28 M. Finšgar and I. Milošev, Inhibition of copper corrosion by 1,2,3-benzotriazole: A review, *Corros. Sci.*, 2010, **52**(9), 2737–2749.
- 29 M. Mehdipour, R. Naderi and B. P. Markhali, Electrochemical study of effect of the concentration of azole



- derivatives on corrosion behavior of stainless steel in H<sub>2</sub>SO<sub>4</sub>, *Prog. Org. Coat.*, 2014, **77**(11), 1761–1767.
- 30 M. G. Cantwell, J. C. Sullivan and R. M. Burgess, Benzotriazoles: History, Environmental Distribution, and Potential Ecological Effects, in *Comprehensive Analytical Chemistry*, Elsevier, 2015, pp. 513–545.
  - 31 M. Petrunin, L. Maksaeva, N. Gladkikh, Y. Makarychev, M. Maleeva and T. Yurasova, *et al.*, Thin Benzotriazole Films for Inhibition of Carbon Steel Corrosion in Neutral Electrolytes, *Coatings*, 2020, **10**(4), 362.
  - 32 H. Dong, M. Chen, S. Rahman, H. S. Parekh, H. M. Cooper and Z. P. Xu, Engineering small MgAl-layered double hydroxide nanoparticles for enhanced gene delivery, *Appl. Clay Sci.*, 2014, **100**, 66–75.
  - 33 S. J. Ko, T. Yamaguchi, F. Salles and J. M. Oh, Systematic utilization of layered double hydroxide nanosheets for effective removal of methyl orange from an aqueous system by  $\pi$ - $\pi$  stacking-induced nanoconfinement, *J. Environ. Manage.*, 2021, **277**, 111455.
  - 34 G. Arrabito, R. Pezzilli, G. Prestopino and P. G. Medaglia, Layered Double Hydroxides in Bioinspired Nanotechnology, *Crystals*, 2020, **10**(7), 602.
  - 35 J. Kameliya, A. Verma, P. Dutta, C. Arora, S. Vyas and R. S. Varma, Layered Double Hydroxide Materials: A Review on Their Preparation, Characterization, and Applications, *Inorganics*, 2023, **11**(3), 121.
  - 36 A. U. Kura, M. Z. Hussein, S. Fakurazi and P. Arulselvan, Layered double hydroxide nanocomposite for drug delivery systems; bio-distribution, toxicity and drug activity enhancement, *Chem. Cent. J.*, 2014, **8**(1), 47.
  - 37 M. Zheludkevich, S. Poznyak, L. Rodrigues, D. Raps, T. Hack and L. Dick, *et al.*, Active protection coatings with layered double hydroxide nanocontainers of corrosion inhibitor, *Corros. Sci.*, 2010, **52**(2), 602–611.
  - 38 M. L. Zheludkevich, J. Tedim and M. G. S. Ferreira, ‘Smart’ coatings for active corrosion protection based on multi-functional micro and nanocontainers, *Electrochim. Acta*, 2012, **82**, 314–323, DOI: [10.1016/j.electacta.2012.04.095](https://doi.org/10.1016/j.electacta.2012.04.095).
  - 39 S. Mallakpour, E. Azadi and C. M. Hussain, Recent advancements in synthesis and drug delivery utilization of polysaccharides-based nanocomposites: The important role of nanoparticles and layered double hydroxides, *Int. J. Biol. Macromol.*, 2021, **193**, 183–204.
  - 40 T. Xu, Q. Y. Wang, J. T. Zhang and J. M. Hu, Electrodeposited graphene/layered double hydroxides micro/nanocontainers for both passive and active corrosion protection, *npj Mater. Degrad.*, 2024, **8**(1), 22.
  - 41 L. Khalili, G. Dehghan, A. Fazli and A. Khataee, State-of-the-art advancement of surface functionalized layered double hydroxides for cell-specific targeting of therapeutics, *Adv. Colloid Interface Sci.*, 2023, **314**, 102869.
  - 42 D. Carneiro, É. P. Damasceno, V. Ferreira, I. Charlie-Silva, J. Tedim and F. Maia, *et al.*, Zn-Al layered double hydroxides induce embryo malformations and impair locomotion behavior in *Danio rerio*, *NanoImpact*, 2023, **30**, 100457.
  - 43 F. Campos, P. V. Silva, A. M. V. M. Soares, R. Martins and S. Loureiro, Harmonizing nanomaterial exposure methodologies in ecotoxicology: the effects of two innovative nanoclays in the freshwater microalgae *Raphidocelis subcapitata*, *Nanotoxicology*, 2023, **17**(5), 401–419.
  - 44 F. Avelas, R. Martins, T. Oliveira, F. Maia, E. Malheiro and A. M. V. M. Soares, *et al.*, Efficacy and ecotoxicity of novel anti-fouling nanomaterials in target and non-target marine species, *Mar. Biotechnol.*, 2017, **19**(2), 164–174.
  - 45 E. Gutner-Hoch, R. Martins, F. Maia, T. Oliveira, M. Shpigel and M. Weis, *et al.*, Toxicity of engineered micro- and nanomaterials with antifouling properties to the brine shrimp *Artemia salina* and embryonic stages of the sea urchin *Paracentrotus lividus*, *Environ. Pollut.*, 2019, **251**, 530–537.
  - 46 R. Martins, J. Figueiredo, A. Sushkova, M. Wilhelm, J. Tedim and S. Loureiro, ‘Smart’ nanosensors for early detection of corrosion: Environmental behavior and effects on marine organisms, *Environ. Pollut.*, 2022, **302**, 118973.
  - 47 A. R. Deip, D. A. Leal, G. H. Sakae, F. Maia, M. A. C. Berton and M. G. S. Ferreira, *et al.*, Performance of commercial LDH traps for chloride ion in a commercial corrosion protection primer for petrochemical industry, *Corros. Eng., Sci. Technol.*, 2020, **55**(1), 66–74.
  - 48 J. Rodriguez, E. Bollen, T. D. Nguyen, A. Portier, Y. Paint and M. G. Olivier, Incorporation of layered double hydroxides modified with benzotriazole into an epoxy resin for the corrosion protection of Zn-Mg coated steel, *Prog. Org. Coat.*, 2020, **149**, 105894.
  - 49 S. Amanian, R. Naderi and M. Mahdavian, Benzotriazole modified Zn-Al layered double hydroxide conversion coating on galvanized steel for improved corrosion resistance, *J. Taiwan Inst. Chem. Eng.*, 2023, **150**, 105072.
  - 50 M. Serdechnova, S. Kallip, M. G. S. Ferreira and M. L. Zheludkevich, Active self-healing coating for galvanically coupled multi-material assemblies, *Electrochem. Commun.*, 2014, **41**, 51–54.
  - 51 S. Bay, R. Burgess and D. Nacci, Status and applications of echinoid (Phylum Echinodermata) toxicity test methods, in *Environmental Toxicology and Risk Assessment*, ASTM International, 1993, pp. 281–302.
  - 52 P. Radix, M. Léonard, C. Papantoniou, G. Roman, E. Saouter and S. Gallotti-Schmitt, *et al.*, Comparison of four chronic toxicity tests using algae, bacteria, and invertebrates assessed with sixteen chemicals, *Ecotoxicol. Environ. Saf.*, 2000, **47**(2), 186–194.
  - 53 F. Flores, L. S. Stapp, J. van Dam, R. Fisher, S. Kaserzon and A. P. Negri, Toxicity of herbicides to the marine microalgae *Tisochrysis lutea* and *Tetraselmis* sp, *Sci. Rep.*, 2024, **14**(1), 1727.
  - 54 ASTM, ASTM E1218-21(2021), Standard Guide for Conducting Static Toxicity Tests with Microalgae, 2021.
  - 55 ASTM, ASTM E1563-21a(2022), Standard guide for conducting short-term chronic toxicity tests with echinoid embryos, 2022.



- 56 J. Figueiredo, T. Oliveira, V. Ferreira, A. Sushkova, S. Silva and D. Carneiro, *et al.*, Toxicity of innovative anti-fouling nano-based solutions to marine species, *Environ. Sci.:Nano*, 2019, **6**, 1418–1429.
- 57 S. Yang, R. S. S. Wu and R. Y. C. Kong, Biodegradation and enzymatic responses in the marine diatom *Skeletonema costatum* upon exposure to 2,4-dichlorophenol, *Aquat. Toxicol.*, 2002, **59**(3–4), 191–200.
- 58 European Commission, *Technical Guidance Document on Risk Assessment*, 2003.
- 59 X. Hou, L. Gao, Z. Cui and J. Yin, Corrosion and Protection of Metal in the Seawater Desalination, *IOP Conf. Ser.: Earth Environ. Sci.*, 2018, **108**, 022037.
- 60 C. Monticelli, Corrosion Inhibitors, in *Encyclopedia of Interfacial Chemistry*, Elsevier, 2018, pp. 164–171.
- 61 K. Auepattana-Aumrung, T. Phakkeeree and D. Crespy, Polymer-corrosion inhibitor conjugates as additives for anticorrosion application, *Prog. Org. Coat.*, 2022, **163**, 106639.
- 62 M. Albini, P. Letardi, L. Mathys, L. Brambilla, J. Schröter and P. Junier, *et al.*, Comparison of a bio-based corrosion inhibitor versus benzotriazole on corroded copper surfaces, *Corros. Sci.*, 2018, **143**, 84–92.
- 63 M. A. Iqbal, C. Neves, M. Starykevich, R. Martins, M. G. S. Ferreira and J. Tedim, In situ grown gluconate-containing CaAl-LDH/organic coating for steel corrosion protection, *J. Coat. Technol. Res.*, 2025, **22**(2), 619–630.
- 64 M. Serdechnova, A. N. Salak, F. S. Barbosa, D. E. L. Vieira, J. Tedim and M. L. Zheludkevich, *et al.*, Interlayer intercalation and arrangement of 2-mercaptobenzothiazolate and 1,2,3-benzotriazolate anions in layered double hydroxides: In situ X-ray diffraction study, *J. Solid State Chem.*, 2016, **233**, 158–165.
- 65 J. Huo, X. Min, Q. Dong, S. Xu and Y. Wang, Comparison of Zn–Al and Mg–Al layered double hydroxides for adsorption of perfluorooctanoic acid, *Chemosphere*, 2022, **287**, 132297.
- 66 C. Wei, X. Yan, Y. Zhou, W. Xu, Y. Gan and Y. Zhang, *et al.*, Morphological Control of Layered Double Hydroxides Prepared by Co-Precipitation Method, *Crystals*, 2022, **12**(12), 1713.
- 67 W. Yu, N. Du, Y. Gu, J. Yan and W. Hou, Specific ion effects on the colloidal stability of layered double hydroxide single-layer nanosheets, *Langmuir*, 2020, **36**(23), 6557–6568.
- 68 F. Varenne, J. B. Coty, J. Botton, F. X. Legrand, H. Hillaireau and G. Barratt, *et al.*, Evaluation of zeta potential of nanomaterials by electrophoretic light scattering: Fast field reversal versus Slow field reversal modes, *Talanta*, 2019, **205**, 120062.
- 69 J. Wu, Q. Ye, P. Wu, S. Xu, Y. Liu and Z. Ahmed, *et al.*, Heteroaggregation of nanoplastics with oppositely charged minerals in aquatic environment: Experimental and theoretical calculation study, *Chem. Eng. J.*, 2022, **428**, 131191.
- 70 D. Takács, T. Szabó, A. Jamnik, M. Tomšič and I. Szilágyi, Colloidal Interactions of Microplastic Particles with Anionic Clays in Electrolyte Solutions, *Langmuir*, 2023, **39**(36), 12835–12844.
- 71 T. L. P. Galvão, C. S. Neves, A. P. F. Caetano, F. Maia, D. Mata and E. Malheiro, *et al.*, Control of crystallite and particle size in the synthesis of layered double hydroxides: Macromolecular insights and a complementary modeling tool, *J. Colloid Interface Sci.*, 2016, **468**, 86–94.
- 72 L. A. Golding, B. M. Angel, G. E. Batley, S. C. Apte, R. Krassoi and C. J. Doyle, Derivation of a water quality guideline for aluminium in marine waters, *Environ. Toxicol. Chem.*, 2015, **34**(1), 141–151.
- 73 M. L. Gillmore, L. A. Golding, B. M. Angel, M. S. Adams and D. F. Jolley, Toxicity of dissolved and precipitated aluminium to marine diatoms, *Aquat. Toxicol.*, 2016, **174**, 82–91.
- 74 G. Pagano, E. His, R. Beiras, A. De Biase, L. G. Korkina and M. Iaccarino, *et al.*, Cytogenetic, developmental, and biochemical effects of aluminum, iron, and their mixture in sea urchins and mussels, *Arch. Environ. Contam. Toxicol.*, 1996, **31**(4), 466–474.
- 75 C. Caplat, R. Oral, M. L. Mahaut, A. Mao, D. Barillier and M. Guida, *et al.*, Comparative toxicities of aluminum and zinc from sacrificial anodes or from sulfate salt in sea urchin embryos and sperm, *Ecotoxicol. Environ. Saf.*, 2010, **73**(6), 1138–1143.
- 76 P. A. Dinnel, J. M. Link, Q. J. Stober, M. W. Letourneau and W. E. Roberts, Comparative sensitivity of sea urchin sperm bioassays to metals and pesticides, *Arch. Environ. Contam. Toxicol.*, 1989, **18**(5), 748–755.
- 77 T. K. Baumiller, Crinoid ecological morphology, *Annu. Rev. Earth Planet. Sci.*, 2008, **36**(1), 221–249.
- 78 C. Dazon, C. Taviot-Guého and V. Prévot, Layered double hydroxides: where should research stress on for massive scaling up?, *Mater. Adv.*, 2023, **4**(20), 4637–4645.
- 79 M. Kumar, R. Pratap Singh and P. A. Kumar, The Role of Layered Double Hydroxides in Semiorganic Doped Quantum Materials, *Int. J. Sci. Res.*, 2025, **14**(2), 1581–1589.
- 80 O. Kaczerewska, R. Martins, J. Figueiredo, S. Loureiro and J. Tedim, Environmental behaviour and ecotoxicity of cationic surfactants towards marine organisms, *J. Hazard. Mater.*, 2020, **392**, 122299.
- 81 C. Blaise, Ecotoxicity of selected nano-materials to aquatic organisms, *Environ. Toxicol.*, 2008, **23**(5), 591–598.

